REVIEW ARTICLE
https://doi.org/10.1038/s41566-018-0310-5

nature photonics

Integrated microwave photonics

David Marpaung[1]*, Jianping Yao[2] and José Capmany[3]

Recent advances in photonic integration have propelled microwave photonic technologies to new heights. The ability to interface hybrid material platforms to enhance light–matter interactions has led to the development of ultra-small and high-bandwidth electro-optic modulators, low-noise frequency synthesizers and chip signal processors with orders-of-magnitude enhanced spectral resolution. On the other hand, the maturity of high-volume semiconductor processing has finally enabled the complete integration of light sources, modulators and detectors in a single microwave photonic processor chip and has ushered the creation of a complex signal processor with multifunctionality and reconfigurability similar to electronic devices. Here, we review these recent advances and discuss the impact of these new frontiers for short- and long-term applications in communications and information processing. We also take a look at the future perspectives at the intersection of integrated microwave photonics and other fields including quantum and neuromorphic photonics.

The use of optical devices and techniques to generate, manipulate, transport and measure high-speed radio-frequency (RF) signals, widely known as microwave photonics (MWP; Box 1), has been the focus of intense research activities in recent years[1–5]. The promise of abundant processing bandwidth obtained from upconverting radio-frequencies to optical frequencies, the availability of low-loss optical fibres as a transport medium, and the flexibility in tailoring the RF response over decades of frequency unlike anything achievable by traditional RF systems have been cited as key drivers in the early development of the technology. Landmark demonstrations include, among others, generation of ultra-broadband signals[6,7], distribution and transport of RF over fibre[8], programmable MWP filters[9,10] and a photonics-enhanced radar system[11]. These progresses have subsequently positioned MWP as a prime technology solution to the impending challenges in communications, including the bandwidth bottleneck in communications systems[12] and the Internet of Things, provided that the hurdles of size, reliability and cost effectiveness are overcome. While impressive the abovementioned demonstrations were in bulky systems composed of relatively expensive discrete fibre-optic components, which are sensitive to external perturbations such as vibrations and temperature gradients.

It was thus serendipitous, but essential, that the rise of MWP technology was paralleled by the surge of photonic integration technologies. The convergence of the two fields, aptly termed integrated MWP, soon followed with profound impacts[5,13]. Leveraging photonic integration allowed a dramatic reduction in the footprint of MWP systems with fairly high complexity, making them more comparable to RF circuits. Optical loss in MWP systems is important because an increase in this parameter translates quadratically into RF loss in RF circuits[5]. For these reasons, efforts at the early stages of development of integrated MWP were focused on reducing on-chip losses[14], on integrating as many components as possible in a single chip[15] and to demonstrate device reconfiguration[7,16].

But integrated photonics offers much more than a reduction in footprint and complexity. For example, confining light in the small mode volume enhances its interaction with matter, most of the time through nonlinear optical processes, which resulted in new technological tools for integrated MWP, such as Kerr microresonator combs[17], hybrid organic–plasmonic modulators[18] and on-chip stimulated Brillouin scattering (SBS)[19]. These tools married with entirely new concepts, for example making a universal reconfigurable processor[20], can significantly alter the capabilities of MWP systems to achieve higher performance, including modulation bandwidth, spectral resolution, noise performance and reconfigurability. On the other hand, major advances in chip integration using a single material (monolithic) or multi-materials (hybrid or heterogeneous) have allowed the integration of all the key components of integrated MWP systems in a single chip[21]. The synergies between integration, advanced functionalities and high performance have been the key highlights of the field in recent times.

Here, we review the most recent advances in integrated MWP. We focus on the new technological tools for integrated MWP, as illustrated in Fig. 1, which are derived from recent breakthroughs and advances in integrated optics. These advances have considerably expanded the performance and the scope of the field, allowing intersections with emerging technologies such as quantum photonics, optomechanics and neuromorphic photonics. We also provide a perspective of how these fields can interact as well as the short- and long-term applications of the technology.

Hybrid integration and emerging materials

Material platforms are a key element in integrated MWP. The choice of material will determine the range of functionalities, performance and the size of the devices and systems. At its inception[5], integrated MWP was mainly demonstrated in a diverse range of materials that included GaAs, lithium niobate and doped silica. But for the past 10 years, most of the integrated MWP circuits have been based on three key platforms for monolithic integration: indium phosphide[22], silicon-on-insulator (SOI)[23–25] and silicon nitride[26,27]. Maturity in the fabrication processes of these materials and their availability through cost-sharing initiatives that dramatically reduce the fabrication cost were the two key drivers of this polarization. The strengths and weaknesses of each of these materials are summarized in Box 2. Table 1 provides a comparison of these materials in terms of the technology features and the quality of components and functionality.

[1]Laser Physics and Nonlinear Optics Group, Faculty of Science and Technology, MESA+ Institute for Nanotechnology, University of Twente, Enschede, The Netherlands. [2]School of Electrical Engineering and Computer Science, University of Ottawa, Ottawa, Ontario, Canada. [3]ITEAM Research Institute, Universitat Politècnica de València, Valencia, Spain. *e-mail: d.a.i.marpaung@utwente.nl

Box 1 | Fundamentals of MWP

A canonical MWP system consists of a laser light source, an optical modulator, an optical signal processor and a photodetector. An input RF signal with frequencies f_{RF}, acquired from an antenna or an RF source, modulates the output of an optical source to upconvert its spectrum to optical frequencies. This typically forms a pair of sidebands at frequencies $\nu \pm f_{RF}$, where ν is the central frequency of the optical source. The combined optical signal is then processed by an optical system composed of several photonic devices forming an optical signal processor, which modifies the spectral characteristics of the sidebands. Finally, an optical detector is employed to downconvert the processed sidebands by beating with the optical carrier so the processed RF signal is recovered.

The functionalities that can be carried out using an MWP system include antenna remoting, RF photonic filtering, true-time delay, phase shifting, optical beamforming, arbitrary waveform generation, frequency up- and downconversion, microwave signal generation and frequency measurement. The quality and range of these functionalities are typically dictated by the optical signal processor.

The performance of an MWP system is usually expressed by three key parameters, namely, the link gain, noise figure and the SFDR. The link gain is a measure of the RF-to-RF loss occurring in the system while the noise figure quantifies the degradation of the signal-to-noise ratio in the system. The SFDR considers the RF nonlinearity occurring in the system and measures the range of RF powers that can be accommodated in the system with sufficient signal-to-noise ratio and negligible intermodulation distortion. These parameters are largely influenced by the output power and the intensity noise of the laser source, the insertion loss, half-wave voltage and linearity of the optical modulator, and the power handling and responsivity of the photodetector.

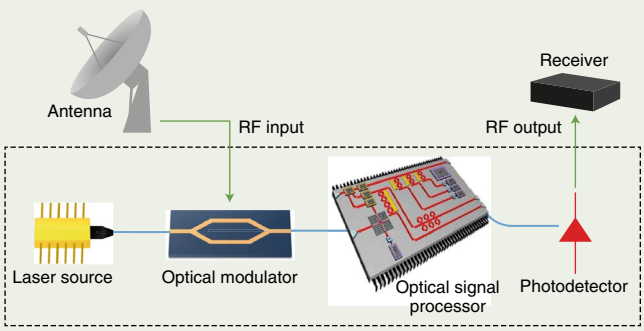

It has been clear for some time that none of these main material platforms can provide all the required performance for integrated MWP on their own. Attempts to create an all-integrated MWP chip in a single platform (in this case indium phosphide) for functionalities such as tunable filters[21] and interference cancellation circuits[28] have been reported with encouraging results, but issues related to waveguide loss and elevated noise due to on-chip amplifiers limit the performance of such circuits. Hence, researchers have turned to a different approach, namely hybrid or heterogeneous integration, to combine different material platforms and to take advantage of their individual strengths. Different approaches have been proposed for this, namely, chip-to-chip (hybrid) integration through vertical or edge coupling[29], or wafer-scale (heterogeneous) integration techniques such as wafer bonding or direct epitaxial growth[30,31] that are more suitable for mass production.

The most rapid advances occurred in the area of III–V integration with silicon or silicon nitride. These circuits were designed to provide reliable light sources and modulators (in III–V semiconductor materials), low-loss circuits (in the case of silicon nitride), or a versatile platform with electronic integration potential in the case of silicon. Hybrid devices have been exploited to show basic and advanced functionalities, such as hybrid metal-oxide–semiconductor (MOS) Mach–Zehnder modulators[32,33], high-gain, high-saturation semiconductor optical amplifiers, and integrated optical and RF sources[29,34]. Integration of multiple materials (silica, silicon nitride, III–V-on-silicon) was recently attempted to create a precise optical frequency synthesizer[35]. Despite these advances consensus has not been reached on which is the most suitable approach for MWP applications since, ideally, simultaneous photonic, RF and complementary metal-oxide–semiconductor (CMOS) electronic compatibility[36] should be targeted.

Apart from the main material platforms discussed above, other material systems have been considered as well for integrated MWP implementation, albeit on a smaller scale and volume, and were focused more on particular light–matter interactions of nonlinear optics, optomechanics and plasmonics. Chalcogenide glass[37] (Fig. 1d), a highly nonlinear material with low two-photon absorption, has mainly been exploited for nonlinear opto-acoustic processing based on Brillouin scattering. Emerging materials such as Hydex[27], Ta_2O_5 (ref. [38]) and aluminium nitride[39] can also be of interest for integrated MWP. Moreover, the availability of the lithium niobate-on-insulator[40] platform has rekindled interest in lithium niobate circuits that have been shown to realize ultra-low-loss waveguides and compact modulators (see section 'Advanced optical modulation'). Finally, 2D materials, especially graphene, on SOI have been proposed for the implementation of high-speed modulators[41], phase shifters, true time delay units and tunable filters[42].

Key functionalities

Functionalities implemented in integrated MWP span optical modulation, generation, processing and measurement of microwave signals. Integration not only brings advantages to these functions, but also enhanced performance. Here, we look at the technological tools that have become available in the past few years that have potentially redefined the field of integrated MWP.

Advanced optical modulation. Optical modulation is the first step in all MWP systems, where the RF signal is encoded in the optical domain. This is a pivotal step that often determines the overall system performance, including bandwidth, system loss, linearity and dynamic range[5]. Typical modulators used in MWP[43] are phase, intensity, or IQ modulators to generate single-sideband modulation or complex modulation with tunable sideband phase and amplitude[19]. In some works, polarization modulators are also utilized[44]. Generally, optical modulation can be achieved through the variation of material absorption (for example in electro-absorption modulators) or through refractive index changes (for example in phase modulators and Mach–Zehnder-type intensity modulators).

For decades, the material of choice for optical modulation has been lithium niobate[45]. In this material, a refractive index change is obtained through the Pockels electro-optic effect. Typical electro-optic lithium niobate modulators are formed either by proton exchange or by the diffusion of titanium, leading to low-index-contrast waveguides with poor optical confinement, which directly leads to high drive voltages and large size. But recent availability of lithium niobate-on-insulator films and improvements in lithium niobate etching techniques have changed this landscape dramatically[46–48]. High-contrast, etched lithium niobate waveguides were recently used to form compact miniaturized lithium niobate modulators a few hundred micrometres in length[46,47] (Fig. 2a). With such a technique, impressive modulator performance was achieved, includ-

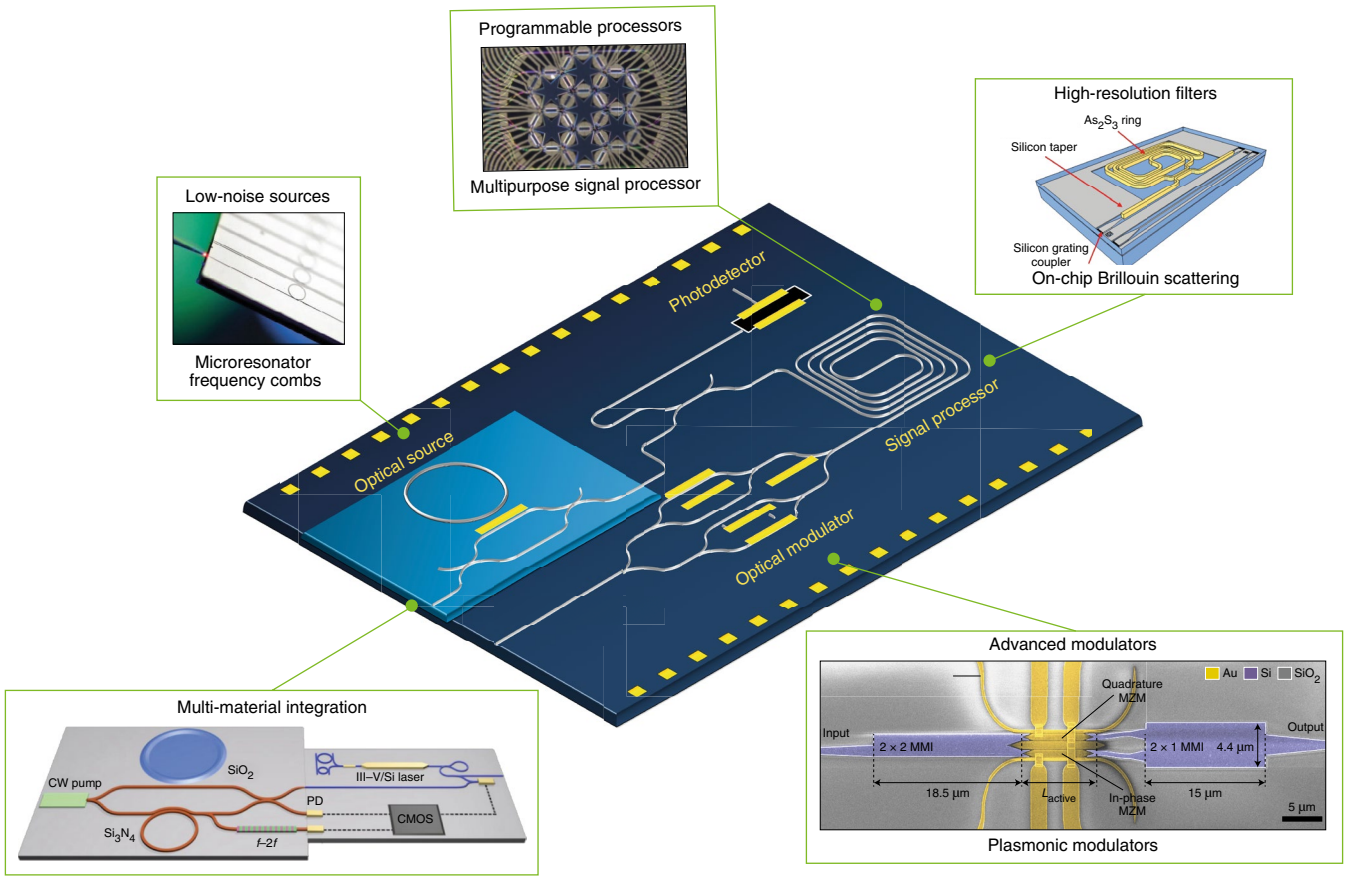

Fig. 1 | Overview of recent advances and technologies in integrated MWP. Kerr microresonator frequency combs can be used as high-quality multiwavelength optical sources for microwave generation and tapped-delay-line microwave photonic filtering. Plasmonic modulators[18] enable ultra-high frequency modulation compatible with silicon platforms and direct RF-to-optical conversion. On-chip Brillouin scattering[84] provides high-resolution filtering unmatched by other on-chip optical filters. A new paradigm of universal programmable processors[98] brings flexibility to MWP and intersects the field with integrated quantum photonics and neuromorphic photonics. Many of these advances are enabled by progresses in hybrid and heterogeneous multi-material integration[35]. CW, continuous wave; MMI, multimode interferometer; *f*–2*f*, frequency doubling. Figure adapted from: programmable processors, ref. [98], under a Creative Commons licence (https://creativecommons.org/licenses/by/4.0/); high-resolution filters, ref. [84], OSA; advanced modulators, ref. [18], IEEE; multi-material integration, ref. [35], Springer Nature Limited. Image of low-noise sources courtesy of the Laboratory of Photonics and Quantum Measurements, EPFL, Swiss Federal Institute of Technology.

ing record-low drive voltage (V_π) of 1.4 V for a single modulator and a bandwidth of 40 GHz in a 20-mm-long modulator[47] (Fig. 2b). The chip insertion loss of the modulator was less than 0.5 dB with 5 dB per facet coupling loss. Higher-frequency operation at 100 GHz was also demonstrated with the $V_\pi L$ figure of merit of 2.2 V cm, where L is the length of the modulator.

Optical modulation has also been explored in silicon, indium phosphide and silicon nitride. The most straightforward way to achieve optical modulation in silicon is to exploit the free-carrier plasma dispersion effect, where changes in the electron and hole densities modify the refractive index and absorption of a silicon waveguide[49]. Modulators based on this effect have shown excellent performance including high-speed operation, but the concept does not allow high performance to be achieved simultaneously with low drive voltage and a small footprint. Optical modulation in the indium phosphide-based platform can be achieved via the quantum-confined Stark effect that induces absorption and refractive index changes[22]. These indium phosphide modulators have shown wide bandwidth beyond 55 GHz (ref. [50]). In silicon nitride, on the other hand, modulation can only be achieved through hybrid integration with indium phosphide[29], 2D materials including graphene[41], or ferroelectric materials such as lead titanate zirconate[51].

Driven by the demand of a high-speed modulator with a small footprint compatible with silicon photonics technology, researchers have proposed a hybrid integration route to combine materials that have a high electro-optic coefficient with strong mode confinement in silicon. In silicon–organic hybrid modulators[52], the strong confinement comes from a silicon slot waveguide, whereas in plasmonic–organic hybrid modulators (Fig. 2c) both optical and RF signals are guided by thin metal sheets, that is, a metal slot waveguide where the light propagates as a surface plasmon polariton mode[18,53–56]. A plasmonic modulator has several advantages over a silicon–organic hybrid modulator, including ultra-short length (tens of micrometres) and higher bandwidth due to ultra-small capacitance. Bandwidth as high as 170 GHz has been achieved with plasmonic devices[55] (Fig. 2d). These modulators have also been seamlessly integrated with an antenna for direct conversion of millimetre waves to the optical domain[56].

While improvements in bandwidth, size and energy consumption are well within reach for a new class of modulator devices, an aspect that is often overlooked is linearity, which is indispensable for analog and RF photonics applications. Linearization of the silicon modulator for analog applications has been explored through heterogeneous integration with lithium niobate[57] or III–V materials[58]

Box 2 | The main material platforms for MWP

Indium phosphide is the only material that enables the monolithic integration of various active and passive photonic components, including lasers, modulators, optical amplifiers, tunable devices and photodetectors, and the platform allows the creation of compact circuits with bending radius of the order of 100 μm. But optical waveguides in this material have relatively high losses of the order of 1.5–3 dB cm^{-1}.

Silicon photonics offers compatibility with microelectronic CMOS fabrication processes making electronic–photonic co-integration a real possibility. Silicon-on-insulator waveguides can exhibit a wide range of losses (0.1–3 dB cm^{-1}) and minimum bending radii (5–100 μm), depending on the thickness of the silicon layer ('thin' ~220 nm or 'thick' ~3 μm) and the geometry of the waveguides (strip or rib). Silicon also shows strong third-order optical nonlinearities, which can be advantageous for ultra-fast signal processing. But the material also suffers from high nonlinear loss through two-photon absorption (TPA) and free-carrier absorption (FCA). Thus silicon is a poor material for light sources, optical modulators, or photodetectors. But through doping, high-speed modulators and photodetectors have been demonstrated.

Silicon nitride waveguides are gaining popularity due to the potential of ultra-low-loss operation. Depending on the deposition method of these layers, post-fabrication processing and geometry, silicon nitride waveguides can be easily tailored to exhibit ultra-low propagation losses (0.01–0.2 dB cm^{-1}), be relatively compact (50–150 μm bending radius), or be able to undergo dispersion engineering necessary for third-order nonlinear processes. The nonlinear coefficient of silicon nitride is about ten times lower compared with silicon. But the low loss and, crucially, the absence of TPA and FCA make it a material of choice for microresonator-based Kerr frequency combs. Lasers, modulators and detectors can be constructed in this passive material only through hybrid integration with other material platforms including indium phosphide, or graphene, or piezoelectric materials.

where the RF third-order nonlinearity term arising from the Mach–Zehnder interferometer transfer function can be cancelled by the nonlinearity of the quantum-confined Stark effect in the III–V material[59] (Fig. 2e). Dynamic range as high as 117 dB $Hz^{2/3}$ has been achieved using such modulators (Fig. 2f).

Low-noise sources and frequency combs. Traditionally, a microwave signal is generated using an electronic oscillator with many stages of frequency doubling to generate a microwave signal with the desired frequency. But with frequency multiplication, the phase noise performance of a microwave signal would be degraded by $10\log_{10}M^2$, where M is the multiplication factor. Microwave photonics, on the other hand, allows direct synthesis of radio-frequencies from the optical domain, opening the path to the generation of very high frequencies with low phase noise.

A straightforward way to optically generate microwaves is to beat the output of two lasers on a photodetector. For example, a microwave synthesizer in a heterogeneously integrated indium phosphide–silicon chip was recently reported[34]. The chip includes a high-speed photodetector, two tunable laser sources and a pair of phase modulators. By tuning the wavelength of one laser source, a microwave signal with a frequency tunable from 1 to 112 GHz was generated. While simple and the frequency tuning is large, the phase terms of the two optical waves are not correlated and the phase noise of the generated microwave signal is high.

Another route to microwave generation is via an optoelectronic oscillator (OEO)[60] that is an MWP link consisting of a laser, a modulator, a high-Q optical cavity and a photodetector with a sustained oscillation through electronic feedback from the detector to the modulator. Numerous schemes to realize an OEO based on discrete components have been reported, but recently, interest in integrated OEOs has peaked. For example, an integrated OEO, where the optical components, including a directly modulated laser source, a spiral-shaped optical delay line and a high-speed photodetector, were fabricated on an indium phosphide substrate was reported[61]. In another approach, integration on a silicon photonic chip using a microdisk resonator as an optical filter was explored[62]. These initial demonstrations, however, were plagued by high phase noise due to the lack of a high-Q resonator as the optical storage element. For example, in ref. [61], the measured phase noise for an output frequency of 7.3 GHz was −91 dBc Hz^{-1} at a 1-MHz offset frequency, which was nearly three orders of magnitude higher compared with an RF electronic oscillator. A key challenge to address then is to integrate an ultra-high-Q cavity[63–65] with the rest of the OEO components.

The most promising technology for pure microwave generation is Kerr frequency combs[63–68]. The beat note generated from the multiple phase-locked harmonics of the combs creates an extremely high spectral purity at a frequency corresponding to the comb spacing. These combs benefit from the division of the noise of the optical source dictated by the ratio of optical to beat note frequencies[68]. Harnessing these combs and other nonlinear effects in resonators, such as Brillouin scattering, has resulted in integrated oscillators with impressive performance. For example, a Kerr optical frequency comb excited in a high-Q magnesium fluoride whispering-gallery-mode resonator was used to generate a microwave signal[68] at 9.9 GHz with a phase noise as low as −120 dBc Hz^{-1} at a 1-kHz offset frequency. In another key demonstration, cascaded Brillouin oscillation on an ultra-high-Q planar silica wedge resonator was used to synthesize 21-GHz microwave signals with a record-low phase-noise floor of −160 dBc Hz^{-1} (ref. [69]). These performances are comparable to that of RF oscillators[69].

Integrated MWP filters. Microwave filtering is one of the most important and fundamental functions in signal processing used to separate information signals from unwanted signals such as noise and interferences. In general, there are two ways of implementing a MWP filter: via a tapped-delay-line architecture, where a number of RF signal copies with well-tailored amplitude and delay profile are summed to form a periodic frequency response, or via a downconverted response of an optical filter response[5,9].

Tapped-delay-line MWP filters typically consist of three key components: a multiwavelength optical source to form the different taps, a spectral shaper for shaping the amplitude and phase of each of the taps, and a dispersive delay line for forming the basic unit delay between the taps, thereby dictating the filter free spectral range[70]. Partial integration of these components has recently been explored (Fig. 3a). Microresonator-based frequency combs have emerged as a powerful tool as a multiwavelength source[71,72]. For example, a Kerr frequency comb containing 45 lines based on a silicon nitride chip was used as an optical source in a single band-pass microwave photonic filter (MPF)[71]. In a similar work, a comb source in Hydex material was used in a tapped-delay-line MPF for Hilbert transformation[72]. In addition, these combs have also been explored as sources for true time delay feeding of phased-array antennas[72]. A pulse shaper has been integrated on an indium phosphide platform to modify the tap weight distribution using a 32-channel arrayed waveguide grating and a dedicated semiconductor optical amplifier for line-by-line control of the channel gain[73]. By exploiting the fast-programmable capability of the pulse shaper, a filter with fast reconfigurability was realized. As for the dispersive delay lines, photonic crystals in III–V materials have been considered as an

Table 1 | Parameters of the main material platforms relevant for MWP

	Silicon-on-insulator	Silicon nitride	Indium phosphide
Refractive index	3.5	2.1	3.1
Waveguide refractive index contrast (%)	>100	>25	10
Bending radius (μm)	5–100	50–150	100
Loss (dB cm^{-1})	0.1–3	0.01–0.2	1.5–3
Nonlinear index (m^2 W^{-1})	4.5×10^{-18}	2.6×10^{-19}	1.5×10^{-17}
Two-photon absorption (cm GW^{-1})	0.25	Negligible	60
Modulator technology (maximum speed)	Free-carrier plasma dispersion (30 GHz)	With graphene (30 GHz) With PZT (33 GHz)	QCSE-EAM (55 GHz)
Detector	Ge (50 GHz)	N/A	40 GHz
Laser output power	N/A	N/A	>20 mW
Fibre-to-chip coupling loss (dB)	2	0.5	3
CMOS compatibility	Excellent	Good	N/A
Optical amplification	N/A	N/A	>20 dB

EAM, electro-absorption modulator; PZT, lead zirconate titanate; QCSE, quantum-confined Stark effect. N/A, not applicable.

integrated replacement for a long length of optical fibre[70]. Despite these progresses, full-circuit integration of the tapped-delay-line filter has never been attempted.

A fully integrated frequency-tunable MPF based on the optical filter response downconversion concept, on the other hand, was recently demonstrated on an indium phosphide platform[21]. All the components, including a laser source, a modulator, an optical filter based on a ring-assisted Mach–Zehnder interferometer and a photodetector, were integrated on a single chip (Fig. 3b). A similar filter demonstration was reported shortly after where a phase modulator, an optical filter based on a microdisk resonator and a photodetector were all integrated in a silicon chip[74].

High-resolution filtering with stimulated Brillouin scattering. Although optical-based RF photonic filters can be tuned over a wide frequency range, the spectral resolution of most optical filters, typically in the gigahertz, is too coarse for processing RF signals where the separation between adjacent information channels can be down to only a few tens of megahertz. Breaking this barrier, a number of integrated MWP filters that combine the strengths of photonic and electronic filters, namely tens of gigahertz frequency tuning with megahertz spectral resolution and an ultra-high extinction, have been reported[19,75–77]. This unique performance metric was achieved by harnessing SBS — a coherent interaction between optical waves and high-frequency acoustic waves (hypersound)[78]. Stimulated Brillouin scattering manifested in the generation of gain and loss resonances with narrow linewidths of the order of 10 MHz.

While SBS has been well studied in long lengths of optical fibres, it has only been observed recently in integrated waveguides[79–83]. Achieving a strong SBS response in integrated waveguides requires material platforms with strong electrostriction and elasto-optic coefficients and large overlap between optical and acoustic modes. To date, the strongest on-chip SBS response was demonstrated in chalcogenide (As_2S_3) waveguides[79,80], while achieving high gain in versatile materials such as silicon is still challenging. Critically, one must combat acoustic phonon leakage from silicon to the silica substrate using suspended structures[81–83]. An alternative approach is to explore heterogeneous integration where a material that supports efficient generation of SBS, such as chalcogenides, is embedded in a CMOS-compatible circuit[84].

On-chip SBS leads to a number of advantages for integrated MWP filters. The ultra-narrow linewidth allows high-resolution filtering unmatched by most on-chip devices. By combining on-chip SBS with a cancellation filter (Fig. 3c), one can simultaneously achieve high resolution with very high stopband rejection of the order of 60 dB while using only 0.8 dB of SBS gain[19] (Fig. 3d). Achieving such an advanced filter using low powers will be important for applications including radar and satellite communications. Another advantage of SBS is all-optical reconfigurability. By pumping the SBS medium not only with a single laser, but with multiple lines with shaped amplitude and frequency spacing, a broadened tailorable response can be achieved and one can generate unique filters with flat-top, sharp-edge frequency response and tunable bandwidth[75]. These devices are promising for channel selections in spectrally crowded RF environments (Fig. 3e).

Programmable signal processing. A major paradigm shift recently occurred in the area of MWP signal processing. To date, most of the reported integrated photonic microwave signal processors have been implemented as application-specific photonic integrated circuits (ASPICs), which are designed to optimally perform a particular MWP functionality[5]. This results in a lack of universality and reconfigurability for multifunctional applications. Leveraging on the strong push towards programmable photonics from related fields, including quantum photonics[85–87], researchers have strived towards programmable and multipurpose integrated MWP devices, with two particular routes explored.

The first approach relies on circuits based on traditional interferometric and photonic waveguide structures designed for flexible programming of its key parameters. Implementation using unit cells of Mach–Zehnder interferometers and ring resonators that can be activated individually, for example, was explored in the context of filtering[16,88], waveform generation[7,89,90], reconfigurable delay lines[15] and frequency measurement[91,92]. More recently, a fully reconfigurable indium phosphide photonic integrated signal processor has been demonstrated[93] made of three active ring resonators and a bypass waveguide as a processing unit cell (Fig. 4a). With this circuit, reconfigurable signal processing functions, including filtering, temporal integration, temporal differentiation and Hilbert transformation, can be performed. Another implementation of this approach includes a photonic signal processor using reconfigurable silicon Bragg gratings[94].

The second approach looks at the possibility of making a generic signal processor from a mesh of uniform tunable building blocks that can be programmed to support multiple functions[20,95–98]. This concept is inspired by field-programmable gate arrays in electronics and by software-defined networks in telecommunications. In two recent demonstrations[20,98], the tunable building block of choice is a

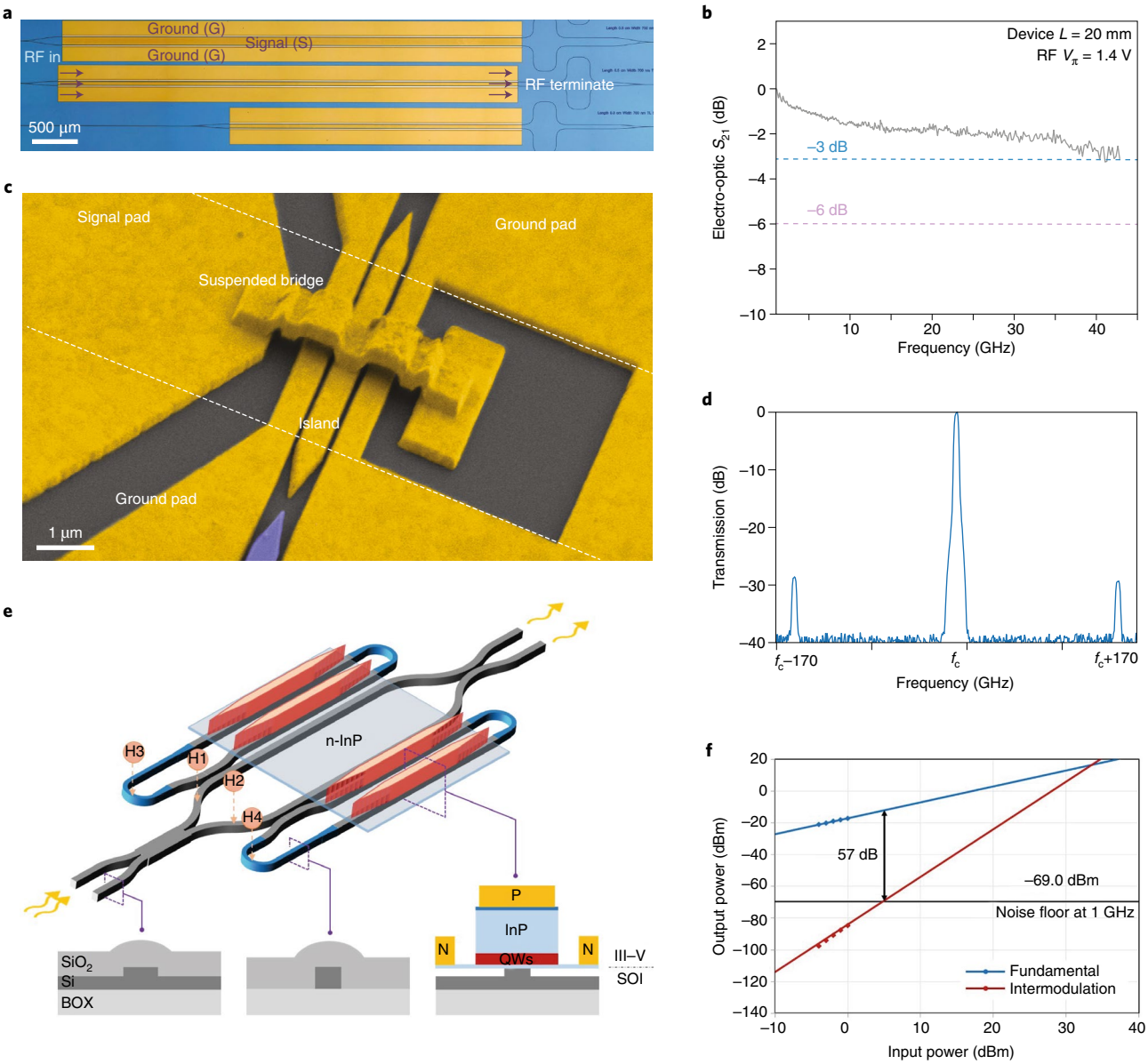

Fig. 2 | Advanced optical modulator technologies for MWP. a, Integrated lithium niobate-on-insulator (LNOI) Mach–Zehnder optical modulator with modulator length of the order of 20 mm (ref. [47]). **b**, The measured electro-optic response of the LNOI modulator. The 20-mm-long device has a 3-dB bandwidth of 40 GHz and an ultra-low RF half-wave voltage of 1.4 V (ref. [47]). **c**, Colorized scanning electron microscopy image of an all-plasmonic Mach–Zehnder modulator. The plasmonic interferometer is formed by the metallic island and the metallic contact pads[53]. **d**, The measured optical spectrum at the output of a plasmonic modulator showing optical sidebands at 170 GHz (ref. [55]). f_c, optical carrier frequency. **e**, Schematic of an ultra-linear optical modulator using a structure of a heterogeneous ring-assisted Mach–Zehnder interferometer (RAMZI) modulator in III-V-on-silicon technology[59]. H1–H4 indicate the locations of the extra thermal phase tuners. BOX, buried oxide. **f**, The measured linearity and SFDR achieved using the ultra-linear heterogeneous RAMZI modulator[59]. SOI, silicon-on-insulator. Figure adapted from: **a**,**b**, ref. [47], Springer Nature Limited; **c**, ref. [53], Springer Nature Limited; **d**, ref. [55], OSA; **e**,**f**, ref. [59], OSA.

Mach–Zehnder interferometer composed of a tunable coupler and four input–output waveguides that can be arranged into a 2D unit cell in square-, triangular-, or hexagonal-type meshes (Fig. 4d). The choice of mesh configuration will determine a number of figures of merit including the spatial tuning resolution step, the number of switching elements per unit area and the losses in the Mach–Zehnder interferometer interconnections. A programmable optical chip connecting Mach–Zehnder interferometer devices in a square-shaped mesh network fabricated in low-loss silicon nitride technology has been reported[20] (Fig. 4b). It consisted of two square cells and was used to demonstrate functionalities including a Hilbert transformer, a delay line, and both notch and bandpass filters (this last functionality is shown in Fig. 4c). A waveguide mesh composed of 7 hexagonal cells fabricated in a silicon platform has also been demonstrated[98]. Figure 4e shows a photograph of the overall structure, which consisted of 30 independent Mach–Zehnder interferometer devices and 60 thermo-optic heaters. The structure is capable of implementing over 100 different circuits and functionalities. Figure 4f shows the optical response of the chip when configured as an add-drop ring resonator.

Several practical issues need attention to advance this processor approach. These include the scaling of the waveguide mesh that is

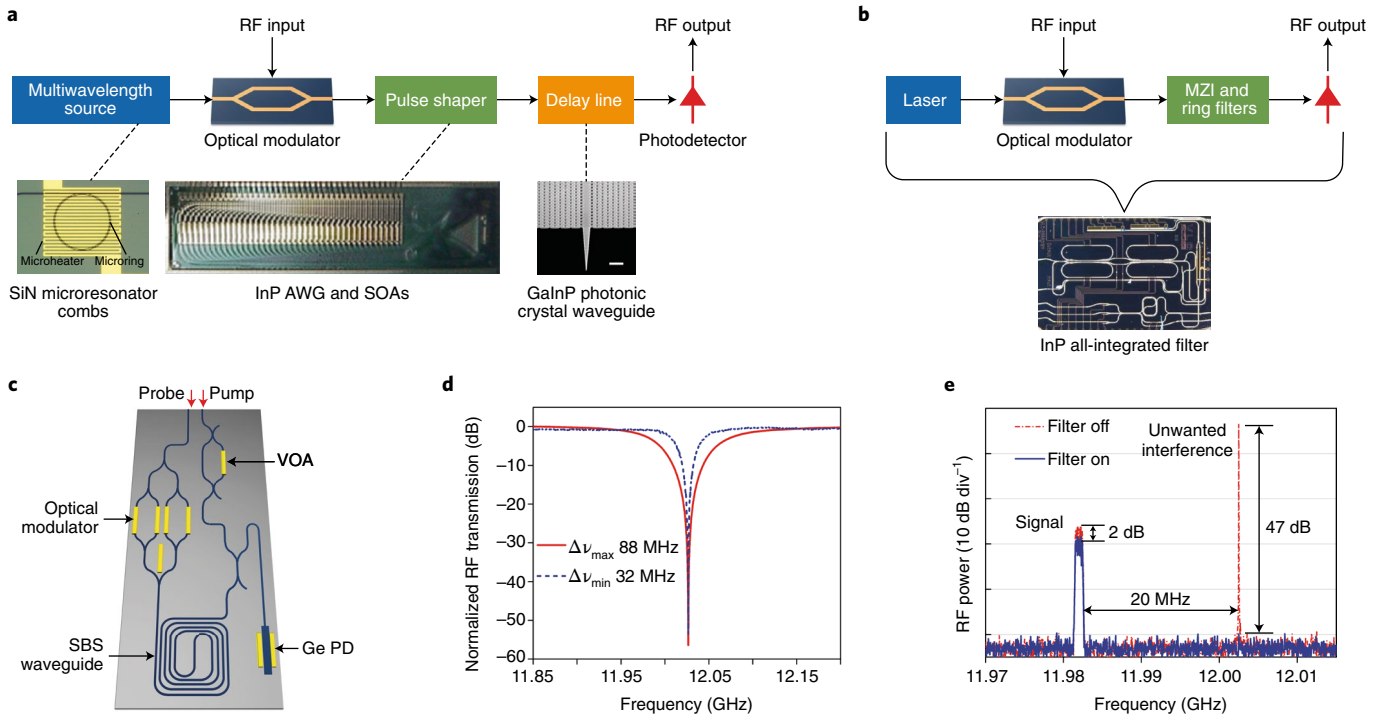

Fig. 3 | Integrated microwave photonic filtering. a, Schematic of a tapped delay line and its integration formed by three key components. Microresonator frequency combs have been used as a multiwavelength source[71]. Line-by-line shaping of each tap has been done using an integrated InP pulse shaper[73]. The dispersive delay lines were miniaturized using GaInP photonic crystal waveguides[70]. Scale bar, 1 μm. AWG, arrayed waveguide grating; SOA, semiconductor optical amplifier. **b**, The microwave photonic filter based on an optical filter has been integrated monolithically on the InP platform[21]. **c**, Artist's impression of an integrated filter based on SBS[19]. PD, photodetector; VOA, variable optical attenuator. **d**, High-resolution RF photonic notch filtering based on a low-power chalcogenide SBS device. The resolution can be tailored from 32 MHz to 88 MHz (ref. [19]). **e**, Filtering of unwanted signal using the SBS filter in **c** and **d**. The unwanted interference 20 MHz away from the desired signal is effectively filtered without significant reduction of the desired signal power[19]. Figure adapted from: **a**(image of microresonator comb), ref. [66], Springer Nature Limited; **a**(image of InP AWG and SOAs), ref. [73], OSA; **a**(image of GaInP photonic crystal waveguide), ref. [70], Springer Nature Limited; **b**(image of InP all-integrated filter), ref. [21], Springer Nature Limited; **c**–**e**, ref. [19], OSA.

directly related to the footprint and loss characteristics of the chosen material platforms, the tracking and stabilization of circuit parameters, the power consumption of the tuning elements, and the operation robustness against fabrication imperfections. Recent works have started to address some of these challenges[99,100].

Challenges

To be deployed in actual RF systems, integrated MWP devices have to achieve comparable performance to RF devices. The requirements in terms of RF characteristics (Box 1) include no loss of the signal of interest (often reflected as zero or positive RF link gain on the decibel scale), a low noise figure below 10 dB and a high spurious-free dynamic range (SFDR) of more than 120 dB $Hz^{2/3}$ (ref. [101]). Such performance has been achieved in analog fibre-optic links for RF signal transport but no other RF photonic processing functionality has been implemented. In contrast, the link performance of reported integrated MWP systems is either well below the required target performance, or, more often, not even considered or reported. If not addressed, the link performance can severely limit the uptake of integrated MWP technologies.

Only recently, researchers have made progress in demonstrating integrated MWP functions simultaneously with high performance. For example, a recent report of a partially integrated MWP filter in silicon nitride showed a positive link gain, a low noise figure of 15.6 dB and a high SFDR of 116 dB $Hz^{2/3}$ (refs. [102,103]) while achieving multiple stopbands with 60 dB extinction. Such a breakthrough in performance was achieved by putting together a number of known approaches for link optimization, including low biasing of a Mach–Zehnder modulator while increasing the input optical power, minimizing the loss in the optical waveguide platform, and using a high-power-handling photodetector composed of multiple photodiodes to ensure linearity. Table 2 compares the filter performance with recent results of integrated and fibre-based[104] MWP filters benchmarked against a high-performance RF filter[105]. It is clear that while MWP filters are competitive or even superior in various figures of merit, the noise figure remains the bottleneck. This is because for passive RF filters, the noise figure is equal to their insertion loss whereas for MWP filters it will be considerably raised by optical noise sources such as relative intensity noise, shot noise and optical amplifier noise.

Extrapolating high link performance to fully integrated systems will be one of the key challenges to address in integrated MWP. This will require efficient and linearized on-chip modulators[58,59], low-loss waveguides[29], high-power and low-noise on-chip lasers[106,107], and high-power-handling photodetectors[108] assembled through heterogeneous integration schemes. For a more detailed discussion on this topic see ref. [109].

Another important challenge to solve for integrated MWP is the power consumption associated with tuning integrated photonics and the signal processing operation. In this regard, alternatives to thermo-optic tuning are needed. Candidates for this include piezoelectrically tuned devices[51]. The use of ultra-low-loss waveguides and resonators in nonlinear materials is also critical to reduce the power threshold of certain nonlinear processes that can lead to ultra-low-power frequency combs[63–65], filters[19] and synthesizers[35], and enable efficient nonlinear integrated MWP signal processing[110].

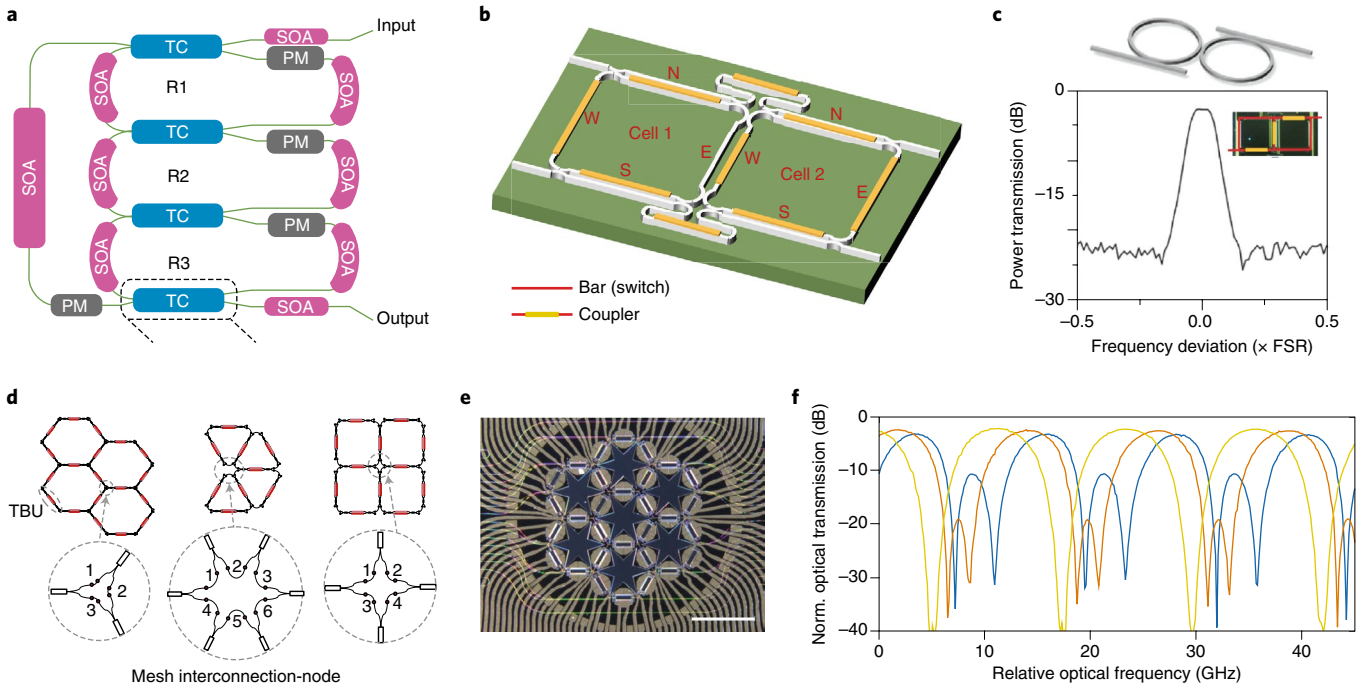

Fig. 4 | Programmable and general-purpose MWP processors. a, Reconfigurable processor in indium phosphide. The device can function as an optical differentiator, integrator and Hilbert transformer[93]. PM, phase modulator; TC, tunable coupler; R1–R3, ring resonators. **b**, A programmable optical chip connecting Mach–Zehnder interferometer devices in a square-shaped mesh network fabricated in low-loss silicon nitride technology[20]. **c**, By thermo-optic tuning, the square-shaped mesh network can be programmed to exhibit a square-shaped bandpass filter normally achieved using a lattice two-ring filter[20]. **d**, Three general topologies of interconnected Mach–Zehnder interferometers, namely triangular, hexagonal and square meshes[97]. TBU, tunable basic unit. **e**, Photograph of a reconfigurable signal processor based on the hexagonal mesh. The overall structure consisted of 30 independent Mach–Zehnder interferometer devices and 60 thermo-optic heaters[98]. Scale bar, 2 mm. **f**, The processor can be programmed to exhibit more than 100 distinct optical responses including an optical response from an add-drop ring resonator[98]. The three curves show central frequency tuning of the optical responses. Figure adapted from: **a**, ref. [93], Springer Nature Limited; **b**,**c**, ref. [20], OSA; **d**, ref. [97], OSA; **e**,**f**, ref. [98], under a Creative Commons licence (https://creativecommons.org/licenses/by/4.0/).

Table 2 | Performance comparison of integrated and fibre-based MWP filters

	Fibre comb-based[104]	Indium phosphide pulse shaper[73]	As_2S_3 SBS[19]	Silicon nitride ring[103]	Indium phosphide MZI and rings[21]	RF resonator[105]
Class	Multi-tap	Multi-tap	Optical filter	Optical filter	Optical filter	Electronic filter
Integration	Not integrated	Partial	Partial	Partial	Full	Full
Type	Bandpass	Bandpass	Bandstop	Bandstop	Lowpass	Bandpass
RF link gain (dB)	0	−3	−30	8	−20	−3.1
Stopband suppression (dB)	32	36	55	50	30	40
Resolution (MHz)	770	130	32	150	5,500	30
Frequency tuning (GHz)	6	2	30	10	4	2.6
Noise figure (dB)	24	N/A	>30	15.6	>30	3.1
SFDR (dB $Hz^{2/3}$)	N/A	N/A	N/A	116	81.4	137

MZI, Mach–Zehnder interferometer. N/A, not applicable.

Outlook and perspectives

Adoption of the technological tools described above has not only equipped MWP with advanced functionalities, but has also expanded the field considerably to allow many intersections with other growing fields in photonics, potentially creating new concepts and paradigms.

The manipulation of phonons and high-frequency sound waves in integrated devices can effectively bridge classical RF photonics processing and cavity optomechanics[111–113] with potential broadened applications from sensing to quantum information science. Architectures that manipulate phonons generated optically and transduced through RF fields hold the promise of enhanced signal processing[111] (Fig. 5a). For example, concepts such as a phononic–photonic emitter–receiver and phonon routing between two opto-mechanical cavities have been used to demonstrate RF photonic bandpass filters with ultra-narrow sub-MHz linewidths[112,113].

Adoption of versatile integrated reconfigurable processors can enable the possibility of multiple input/multiple output (MIMO)

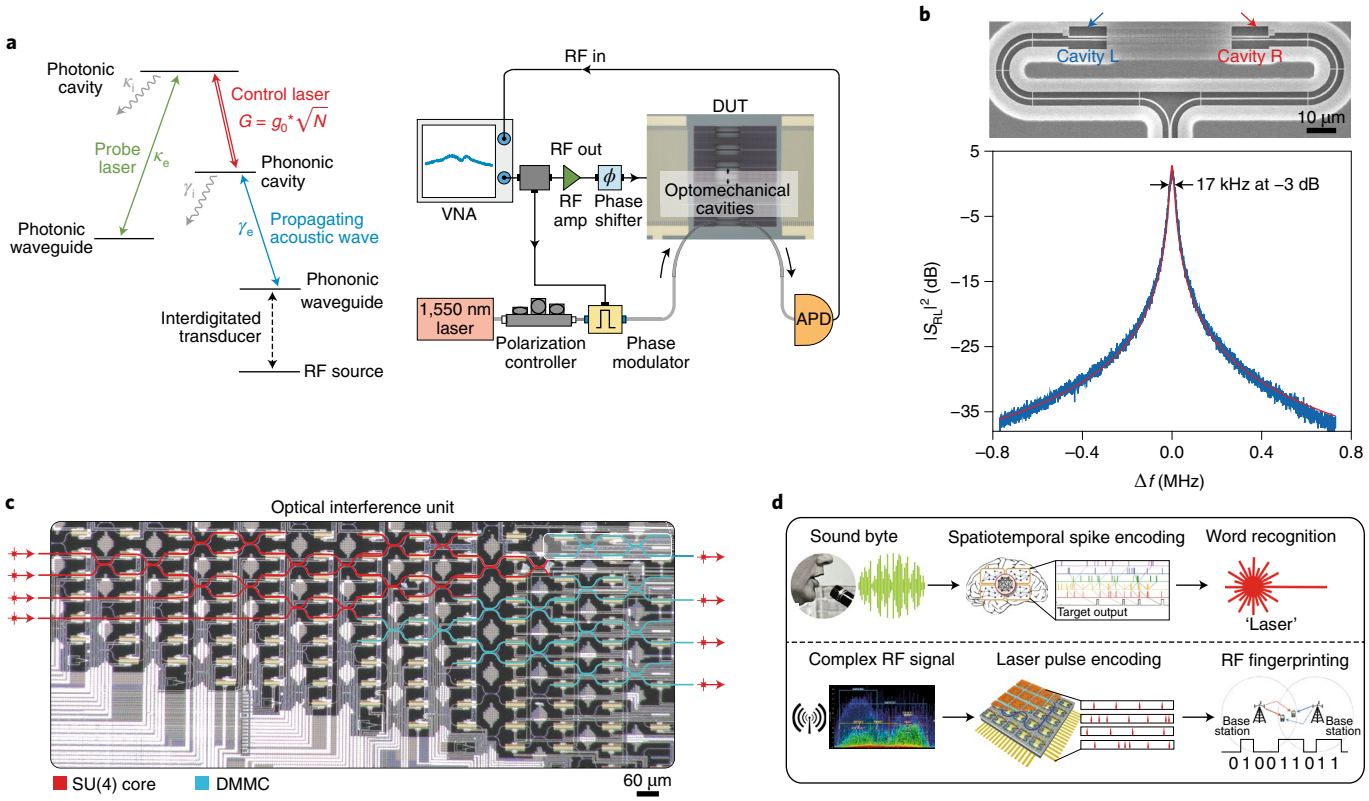

Fig. 5 | Opportunities for integrated MWP. a, High-frequency phonons for bridging RF and photonic domains. An optomechanical device in piezoelectric materials can couple phonons generated from RF sources and phonons generated optically as depicted by the level diagram (left) and the measurement set-up (right)[111]. κ_e, optical cavity coupling rate; κ_i, intrinsic optical cavity decay rate; γ_e, phononic cavity coupling rate; γ_i, intrinsic phononic cavity decay rate; APD, avalanche photodetector; DUT, device under test; VNA, vector network analyser. **b**, An optomechanical structure consisting of two optical microcavities connected by a phononic waveguide (upper) can act as a high-resolution filter with 17-kHz, 3-dB bandwidth (lower)[113]. **c**, Programmable optical processors intersect integrated MWP with emerging fields including integrated quantum photonic and neuromorphic photonics. The figure depicts a programmable nanophotonic processor in silicon photonics used for deep-learning applications. The chip is composed of 56 Mach–Zehnder interferometers, 213 phase shifters and 112 directional couplers[118]. **d**, Illustration of neuromorphic photonic concepts implemented for RF fingerprinting of complex and crowded RF environments for cognitive radio applications[117]. DMMC, diagonal matrix multiplication core. Figure adapted from: **a**, ref. [111], Springer Nature Limited; **b**, ref. [113], Springer Nature Limited; **c**, ref. [118], Springer Nature Limited; **d**, © ref. [117], reproduced by permission of Taylor and Francis Group LLC, a division of Informa plc.

MWP and open the door to parallel linear processing[114] and space-division multiplexing[115,116]. Furthermore, analog photonic principles combined with unitary $N \times N$ transformations have been proposed as a key technology for the implementation of spiking and reservoir neuromorphic photonic systems, deep learning (Fig. 5b) and brain-inspired processing[117–119]. These concepts can be implemented in the wideband fingerprinting of crowded wireless environments for cognitive radio applications[119] (Fig. 5c,d). Interestingly, integrated MWP systems based on cascaded ring modulation by RF signals have also been proposed for the implementation of a new generation of processing systems based on topological photonics[120].

The concept of parity–time symmetry in laser optics to achieve single-mode lasing[121–123] has recently been employed in MWP systems for filterless single-frequency microwave generation. This concept overcomes the long existing problems of mode competition and mode selection that have severely limited the development of OEOs[124,125], particularly in integrated devices where an ultra-narrowband optical filter is difficult to implement.

These concepts in integrated MWP driven by the new understanding in device physics and the tremendous growth of integrated photonics represent a new phase in the field beyond telecom-related applications. Such explorations will sustain the growth of these fields and bring further exciting opportunities.

Received: 31 May 2018; Accepted: 5 October 2018;
Published online: 21 January 2019

References

1. Seeds, A. J. & Williams, K. J. Microwave photonics. *J. Lightw. Technol.* **24**, 4628–4641 (2006).
2. Minasian, R. A. Photonic signal processing of microwave signals. *IEEE Trans. Microw. Theory Tech.* **54**, 832–846 (2006).
3. Capmany, J. & Novak, D. Microwave photonics combines two worlds. *Nat. Photon.* **1**, 319–330 (2007).
4. Yao, J. Microwave photonics. *J. Lightw. Technol.* **27**, 314–335 (2009).
5. Marpaung, D. et al. Integrated microwave photonics. *Laser Photon. Rev.* **7**, 506–538 (2013).
6. Yao, J. P., Zeng, F. & Wang, Q. Photonic generation of ultra-wideband signals. *J. Lightw. Technol.* **25**, 3219–3235 (2007).
7. Khan, M. et al. Ultrabroad-bandwidth arbitrary radiofrequency waveform generation with a silicon photonic chip-based spectral shaper. *Nat. Photon.* **4**, 117–122 (2009).
8. Lim, C. et al. Fiber-wireless networks and subsystem technologies. *J. Lightw. Technol.* **28**, 390–405 (2010).
9. Capmany, J., Ortega, B. & Pastor, D. A tutorial on microwave photonic filters. *J. Lightw. Technol.* **24**, 201–229 (2006).
10. Supradeepa, V. R. et al. Comb-based radiofrequency photonic filters with rapid tunability and high selectivity. *Nat. Photon.* **6**, 186–194 (2012).
11. Ghelfi, P. et al. A fully photonics-based coherent radar system. *Nature* **507**, 341–345 (2014).

12. Hecht, J. The bandwidth bottleneck that is throttling the Internet. *Nature* **536**, 139–142 (2016).
13. Iezekiel, S., Burla, M., Klamkin, J., Marpaung, D. & Capmany, J. RF engineering meets optoelectronics. *IEEE Microw. Mag.* **16**, 18–45 (2015).
14. Zhuang, L. et al. Low-loss high-index-contrast Si_3N_4/SiO_2 optical waveguides for optical delay lines in microwave photonics signal processing. *Opt. Express* **19**, 23162–23170 (2011).
15. Burla, M. et al. On-chip CMOS compatible reconfigurable optical delay line with separate carrier tuning for microwave photonic signal processing. *Opt. Express* **19**, 21475–21484 (2011).
16. Norberg, E. J., Guzzon, R. S., Parker, J. S., Johansson, L. A. & Coldren, L. A. Programmable photonic microwave filters monolithically integrated in InP/InGaAsP. *J. Lightw. Technol.* **29**, 1611–1619 (2011).
17. Kippenberg, T. J., Holzwarth, R. & Diddams, S. A. Microresonator-based optical frequency combs. *Science* **332**, 555–559 (2011).
18. Haffner, C. et al. Plasmonic organic hybrid modulators—scaling highest speed photonics to the microscale. *Proc. IEEE* **104**, 2362–2379 (2016).
19. Marpaung, D. et al. Low power, chip-based stimulated Brillouin scattering microwave photonic filter with ultrahigh selectivity. *Optica* **2**, 76–83 (2015).
20. Zhuang, L., Roeloffzen, C. G. H., Hoekman, M., Boller, K. J. & Lowery, A. J. Programmable photonic signal processor chip for radiofrequency applications. *Optica* **2**, 854–859 (2015).
21. Fandiño, J. S., Muñoz, P., Doménech, D. & Capmany, J. A monolithic integrated photonic microwave filter. *Nat. Photon.* **11**, 124–129 (2016).
22. Smit, M. et al. An introduction to InP-based generic integration technology. *Semicond. Sci. Technol.* **29**, 083001 (2014).
23. Thomson, D. et al. Roadmap on silicon photonics. *J. Opt.* **18**, 073003 (2016).
24. Zhang, W. & Yao, J. Silicon-based integrated microwave photonics. *IEEE J. Quantum Electron.* **52**, 0600412 (2016).
25. Leuthold, J., Koos, C. & Freude, W. Nonlinear silicon photonics. *Nat. Photon.* **4**, 535–544 (2010).
26. Roeloffzen, C. H. G. et al. Silicon nitride microwave photonic circuits. *Opt. Express* **21**, 22937–22961 (2013).
27. Moss, D. J., Morandotti, R., Gaeta, A. L. & Lipson, M. New CMOS-compatible platforms based on silicon nitride and Hydex for nonlinear optics. *Nat. Photon.* **7**, 597–607 (2013).
28. Chang, M. P., Blow, E. C., Lu, M. Z., Sun, J. J. & Prucnal, P. R. Integrated microwave photonic circuit for self-interference cancellation. *IEEE Trans. Microw. Theory Tech.* **65**, 4493–4501 (2017).
29. Roeloffzen, C. G. H. et al. Low-loss Si_3N_4 TriPleX optical waveguides: technology and applications overview. *IEEE J. Sel. Top. Quantum Electron.* **24**, 4400321 (2018).
30. Heck, M. J. R. et al. Hybrid silicon photonic integrated circuit technology. *IEEE J. Quantum Electron.* **19**, 6100117 (2013).
31. Komljenovic, T. et al. Heterogeneous silicon photonic integrated circuits. *J. Lightw. Technol.* **34**, 20–35 (2016).
32. Hiraki, T. et al. Heterogeneously integrated III–V/Si MOS capacitor Mach–Zehnder modulator. *Nat. Photon.* **11**, 482–485 (2017).
33. Han, J. H. et al. Efficient low-loss InGaAsP/Si hybrid MOS optical modulator. *Nat. Photon.* **11**, 486–490 (2017).
34. Hulme, J. et al. Fully integrated microwave frequency synthesizer on heterogeneous silicon-III/V. *Opt. Express* **25**, 2422–2431 (2017).
35. Spencer, D. T. et al. An integrated-photonics optical-frequency synthesizer. *Nature* **557**, 81–85 (2018).
36. Sun, C. et al. Single-chip microprocessor that communicates directly using light. *Nature* **528**, 534–538 (2015).
37. Eggleton, B. J., Luther-Davies, B. & Richardson, K. Chalcogenide photonics. *Nat. Photon.* **5**, 141–148 (2011).
38. Belt, M., Davenport, M., Bowers, J. & Blumenthal, D. Ultra-low-loss Ta_2O_5-core/SiO_2-clad planar waveguides on Si substrates. *Optica* **4**, 532–536 (2017).
39. Xiong, C., Pernice, W. H. P. & Tang, H. X. Low-loss silicon integrated aluminum nitride photonic circuits and their use for electro-optic signal processing. *Nano Lett.* **12**, 3562–3568 (2012).
40. Zhang, M., Wang, C., Cheng, R., Shams-Ansari, A. & Lončar, M. Monolithic ultra-high-*Q* lithium niobate microring resonator. *Optica* **4**, 1536–1537 (2017).
41. Phare, C. T., Daniel Lee, Y.-H., Cardenas, J. & Lipson, M. Graphene electro-optic modulator with 30 GHz bandwidth. *Nat. Photon.* **9**, 511–514 (2015).
42. Capmany, J., Doménech, D. & Muñoz, P. Graphene integrated microwave photonics. *J. Lightw. Technol.* **32**, 3785–3796 (2014).
43. Li, G. L. & Yu, P. K. L. Optical intensity modulators for digital and analog applications. *J. Lightw. Technol.* **21**, 2010–2030 (2003).
44. Bull, J. D. et al. 40 GHz electro-optic polarization modulator for fiber optic communications systems. *Proc. SPIE* **5577**, 133–143 (2004).
45. Wooten, E. L. et al. A review of lithium niobate modulators for fiber-optic communications systems. *IEEE J. Sel. Top. Quantum Electron.* **6**, 69–82 (2000).
46. Wang, C., Zhang, M., Stern, B., Lipson, M. & Loncar, M. Nanophotonic lithium niobate electro-optic modulators. *Opt. Express* **26**, 1547–1555 (2018).
47. Wang, C. et al. Integrated lithium niobate electro-optic modulators operating at CMOS-compatible voltages. *Nature* **562**, 101–104 (2018).
48. Rao, A. & Fathpour, S. Compact lithium niobate electrooptic modulators. *IEEE J. Sel. Top. Quantum Electron.* **24**, 3400114 (2018).
49. Soref, R. A. & Bennett, B. R. Electrooptical effects in silicon. *IEEE J. Quantum Electron.* **23**, 123–129 (1987).
50. Trajkovic, M. et al. 55 GHz EAM bandwidth and beyond in InP active-passive photonic integration platform. In *Proc. CLEO* Paper JTh5A.8 (OSA, 2018).
51. Alexander, K. et al. Nanophotonic Pockels modulators on a silicon nitride platform. *Nat. Commun.* **9**, 3444 (2018).
52. Koos, C. et al. Silicon-organic hybrid (SOH) and plasmonic-organic hybrid (POH) integration. *J. Lightw. Technol.* **34**, 256–268 (2016).
53. Haffner, C. et al. All-plasmonic Mach–Zehnder modulator enabling optical high-speed communication at the microscale. *Nat. Photon.* **9**, 525–528 (2015).
54. Ayata, M. et al. High-speed plasmonic modulator in a single metal layer. *Science* **358**, 630–632 (2017).
55. Hoessbacher, C. et al. Plasmonic modulator with >170 GHz bandwidth demonstrated at 100 GBd NRZ. *Opt. Express* **25**, 1762–1768 (2017).
56. Salamin, Y. et al. Direct conversion of free space millimeter waves to optical domain by plasmonic modulator antenna. *Nano Lett.* **15**, 8342–8346 (2015).
57. Chen, L., Chen, J., Nagy, J. & Reano, R. M. Highly linear ring modulator from hybrid silicon and lithium niobate. *Opt. Express* **23**, 13255–13264 (2015).
58. Zhang, C., Morton, P. A., Khurgin, J. B., Peters, J. D. & Bowers, J. E. Highly linear heterogeneous-integrated Mach–Zehnder interferometer modulators on Si. *Opt. Express* **24**, 19040–19047 (2016).
59. Zhang, C., Morton, P. A., Khurgin, J. B., Peters, J. D. & Bowers, J. E. Ultralinear heterogeneously integrated ring assisted Mach–Zehnder interferometer modulator on silicon. *Optica* **3**, 1483–1488 (2016).
60. Maleki, L. Sources: the optoelectronic oscillator. *Nat. Photon.* **5**, 728–730 (2011).
61. Tang, J. et al. Integrated optoelectronic oscillator. *Opt. Express* **26**, 12257–12265 (2018).
62. Zhang, W. & Yao, J. Silicon photonic integrated optoelectronic oscillator for frequency-tunable microwave generation. *J. Lightw. Technol.* **36**, 4655–4663 (2018).
63. Yang, K. Y. et al. Bridging ultrahigh-*Q* devices and photonic circuits. *Nat. Photon.* **12**, 297–302 (2018).
64. Ji, X. et al. Ultra-low-loss on-chip resonators with sub-milliwatt parametric oscillation threshold. *Optica* **4**, 619–624 (2017).
65. Xuan, Y. et al. High-*Q* silicon nitride microresonators exhibiting low-power frequency comb initiation. *Optica* **3**, 1171–1180 (2016).
66. Xue, X. et al. Mode-locked dark pulse Kerr combs in normal-dispersion microresonators. *Nat. Photon.* **9**, 594–600 (2015).
67. Marin-Palomo, P. et al. Microresonator-based solitons for massively parallel coherent optical communications. *Nature* **546**, 274–279 (2017).
68. Liang, W. et al. High spectral purity Kerr frequency comb radio frequency photonic oscillator. *Nat. Commun.* **6**, 7957 (2015).
69. Li, J., Lee, H. & Vahala, K. J. Microwave synthesizer using an on-chip Brillouin oscillator. *Nat. Commun.* **4**, 2097 (2013).
70. Sancho, J. et al. Integrable microwave filter based on a photonic crystal delay line. *Nat. Commun.* **3**, 1075 (2012).
71. Xue, X. et al. Programmable single-bandpass photonic RF filter based on Kerr comb from a microring. *J. Lightw. Technol.* **32**, 3557–3565 (2014).
72. Wu, J. et al. RF photonics: an optical microcombs' perspective. *IEEE J. Sel. Top. Quantum Electron.* **24**, 6101020 (2018).
73. Metcalf, A. J. et al. Integrated line-by-line optical pulse shaper for high-fidelity and rapidly reconfigurable RF-filtering. *Opt. Express* **24**, 23925–23940 (2016).
74. Zhang, W. & Yao, J. On-chip silicon photonic integrated frequency-tunable bandpass microwave photonic filter. *Opt. Lett.* **43**, 3622–3625 (2018).
75. Choudhary, A. et al. Tailoring of the Brillouin gain for on-chip widely tunable and reconfigurable broadband microwave photonic filters. *Opt. Lett.* **41**, 436–439 (2016).
76. Aryanfar, I. et al. Signal interference RF photonic bandstop filter. *Opt. Express* **24**, 14995–15004 (2016).
77. Morrison, B. et al. Tunable microwave photonic notch filter using on-chip stimulated Brillouin scattering. *Opt. Commun.* **313**, 85–89 (2014).
78. Eggleton, B. J., Poulton, C. G. & Pant, R. Inducing and harnessing stimulated Brillouin scattering in photonic integrated circuits. *Adv. Opt. Photon.* **5**, 536–587 (2013).
79. Pant, R. et al. On-chip stimulated Brillouin scattering. *Opt. Express* **19**, 8285–8290 (2011).
80. Choudhary, A. et al. Advanced integrated microwave signal processing with giant on-chip Brillouin gain. *J. Lightw. Technol.* **35**, 846–854 (2017).
81. Shin, H. et al. Tailorable stimulated Brillouin scattering in nanoscale silicon waveguides. *Nat. Commun.* **4**, 1944 (2013).
82. Laer, R. V., Kuyken, B., Thourhout, D. V. & Baets, R. Interaction between light and highly confined hypersound in a silicon photonic nanowire. *Nat. Photon.* **9**, 199–203 (2015).

83. Kittlaus, E. A., Shin, H. & Rakich, P. T. Large Brillouin amplification in silicon. *Nat. Photon.* **10**, 463–467 (2016).
84. Morrison, B. et al. Compact Brillouin devices through hybrid integration on silicon. *Optica* **4**, 847–854 (2017).
85. Carolan, J. et al. Universal linear optics. *Science* **349**, 711–716 (2015).
86. Harris, N. C. et al. Quantum transport simulations in a programmable nanophotonic processor. *Nat. Photon.* **11**, 447–452 (2017).
87. Wang, J. et al. Multidimensional quantum entanglement with large-scale integrated optics. *Science* **360**, 285–291 (2018).
88. Ibrahim, S. et al. Demonstration of a fast-reconfigurable silicon CMOS optical lattice filter. *Opt. Express* **19**, 13245–13256 (2011).
89. Marpaung, D., Chevalier, L., Burla, M. & Roeloffzen, C. Impulse radio ultrawideband pulse shaper based on a programmable photonic chip frequency discriminator. *Opt. Express* **19**, 24838–24848 (2011).
90. Wang, J. et al. Reconfigurable radio-frequency arbitrary waveforms synthesized in a silicon chip. *Nat. Commun.* **6**, 5957 (2015).
91. Marpaung, D. On-chip photonic-assisted instantaneous microwave frequency measurement system. *IEEE Photon. Technol. Lett.* **25**, 837–840 (2013).
92. Fandiño, J. S. & Muñoz, P. Photonics-based microwave frequency measurement using a double-sideband suppressed-carrier modulation and an InP integrated ring-assisted Mach–Zehnder interferometer filter. *Opt. Lett.* **38**, 4316–4319 (2013).
93. Liu, W. et al. A fully reconfigurable photonic integrated signal processor. *Nat. Photon.* **10**, 190–195 (2016).
94. Zhang, W. & Yao, J. A fully reconfigurable waveguide Bragg grating for programmable photonic signal processing. *Nat. Commun.* **9**, 1396 (2018).
95. Pérez, D., Gasulla, I. & Capmany, J. Software-defined reconfigurable microwave photonics processor. *Opt. Express* **23**, 14640–14654 (2015).
96. Capmany, J., Gasulla, I. & Pérez, D. Microwave photonics: the programmable processor. *Nat. Photon.* **10**, 6–8 (2016).
97. Pérez, D., Gasulla, I., Capmany, J. & Soref, R. A. Reconfigurable lattice mesh designs for programmable photonic processors. *Opt. Express* **24**, 12093–12106 (2016).
98. Pérez, D. et al. Multipurpose silicon photonics signal processor core. *Nat. Commun.* **8**, 636 (2017).
99. Miller, D. A. B. Perfect optics with imperfect components. *Optica* **2**, 747–750 (2015).
100. Grillanda, S. et al. Non-invasive monitoring and control in silicon photonics using CMOS integrated electronics. *Optica* **1**, 129–136 (2014).
101. Urick, V. J., McKinney, J. D. & Williams, K. J. *Fundamentals of Microwave Photonics* (John Wiley & Sons, Hoboken, NJ, 2015).
102. Liu, Y., Marpaung, D., Choudhary, A. & Eggleton, B. J. Lossless and high-resolution RF photonic notch filter. *Opt. Lett.* **41**, 5306–5309 (2016).
103. Liu, Y., Hotten, J., Choudhary, A., Eggleton, B. J. & Marpaung, D. All-optimized integrated RF photonic notch filter. *Opt. Lett.* **42**, 4631–4634 (2017).
104. Kim, H. J., Leaird, D. E., Metcalf, A. J. & Weiner, A. M. Comb-based RF photonic filters based on interferometric configuration and balanced detection. *J. Lightw. Technol.* **32**, 3478–3488 (2014).
105. Joshi, H., Sigmarsson, H., Moon, S., Peroulis, D. & Chappell, W. J. High-*Q* fully reconfigurable tunable bandpass filters. *IEEE Trans. Microw. Theory Tech.* **57**, 3525–3533 (2009).
106. Fan, Y. et al. 290 Hz intrinsic linewidth from an integrated optical chip based widely tunable InP-Si_3N_4 hybrid laser. In *Proc. CLEO* Paper JTh5C.9 (OSA, 2017).
107. Morton, P., Morton, M. & Morton, S. Ultra low phase noise, high power, hybrid lasers for RF mixing and optical sensing applications. In *Proc. IEEE Avionics and Vehicle Fiber-Optics Photon. Conf. (AVFOP)* Paper TuB.1 (IEEE, 2017).
108. Beling, A., Xie, X. & Campbell, J. C. High-power, high-linearity photodiodes. *Optica* **3**, 328–338 (2016).
109. Liu, Y., Marpaung, D., Choudhary, A., Hotten, J. & Eggleton, B. J. Link performance optimization of chip-based Si_3N_4 microwave photonic filters. *J. Lightw. Technol.* **36**, 4361–4370 (2018).
110. Marpaung, D., Pagani, M., Morrison, B. & Eggleton, B. J. Nonlinear integrated microwave photonics. *J. Lightw. Technol.* **32**, 3421–3427 (2014).
111. Balram, K. C., Davanço, M. I., Song, J. D. & Srinivasan, K. Coherent coupling between radiofrequency, optical and acoustic waves in piezo-optomechanical circuits. *Nat. Photon.* **10**, 346–352 (2016).
112. Kittlaus, E. A. RF-photonic filters via on-chip photonic–phononic emit–receive operations. *J. Lightw. Technol.* **36**, 2803–2809 (2018).
113. Fang, K., Matheny, M. H., Luan, X. & Painter, O. Optical transduction and routing of microwave phonons in cavity-optomechanical circuits. *Nat. Photon.* **10**, 489–496 (2016).
114. Perez, D. et al. Silicon photonics rectangular universal interferometer. *Laser Photon. Rev.* **11**, 1700219 (2017).
115. Wen, H. et al. Few-mode fibre-optic microwave photonic links. *Light Sci. Appl.* **6**, e17021 (2017).
116. Annoni, A. et al. Unscrambling light—automatically undoing strong mixing between modes. *Light Sci. Appl.* **6**, e17110 (2017).
117. Prucnal, P. R. & Shastri, B. J. *Neuromorphic Photonics* (CRC Press, Boca Raton, 2017).
118. Shen, Y. C. et al. Deep learning with coherent nanophotonic circuits. *Nat. Photon.* **11**, 441–446 (2017).
119. Cheng, Z., Rios, C., Pernice, W. H., Wright, C. D. & Bhaskaran, H. On-chip photonic synapse. *Sci. Adv.* **3**, e1700160 (2017).
120. Ozawa, T., Price, H. M., Goldman, N., Zilberberg, O. & Carusotto, I. Synthetic dimensions in integrated photonics: from optical isolation to four-dimensional quantum Hall physics. *Phys. Rev. A* **93**, 043827 (2016).
121. Feng, L., Wong, Z. J., Ma, R. M., Wang, Y. & Zhang, X. Single-mode laser by parity-time symmetry breaking. *Science* **346**, 972–975 (2014).
122. Hodaei, H., Miri, M. A., Heinrich, M., Christodoulides, D. N. & Khajavikhan, M. Parity-time–symmetric microring lasers. *Science* **346**, 975–978 (2014).
123. Liu, W. et al. An integrated parity-time symmetric wavelength-tunable single-mode microring laser. *Nat. Commun.* **8**, 15389 (2017).
124. Zhang, J. & Yao, J. Parity-time symmetric optoelectronic oscillator. *Sci. Adv.* **4**, eaar6782 (2018).
125. Liu, Y. et al. Observation of parity-time symmetry in microwave photonics. *Light Sci. Appl.* **7**, 38 (2018).

Acknowledgements

D.M. wishes to acknowledge funding from NWO-TTW Vidi 15702. The work of J.Y. is supported by the Natural Sciences and Engineering Research Council of Canada. J.C. wishes to acknowledge funding from ERC ADG-2016-741415 UMWP-CHIP, GVA PROMETEO 2017/103 and COST CA16220 EUIMWP.

Competing interests

The authors declare no competing interests.

Additional information

Reprints and permissions information is available at www.nature.com/reprints.

Correspondence should be addressed to D.M.

Publisher's note: Springer Nature remains neutral with regard to jurisdictional claims in published maps and institutional affiliations.